WITHDRAWN ARTICLE

WITHDRAWN: Macrophage-targeting Fasudil treatment protects liver from the ischemia/reperfusion injury by promoting M2 macrophage polarization

Yingli Xie ; Di Zhao ; Pingshuan Dong ; Lihong Lai

Biosci Rep (2021) BSR20171734; **DOI:** 10.1042/BSR20171734

The Accepted Manuscript version of this article (published on 12 February 2018) was withdrawn on 9 April 2021 at the request of the authors. Despite numerous attempts to contact the authors, the Editorial Office have been unable to receive a reason behind the withdrawal request.

Title: Macrophage-targeting Fasudil treatment protects liver from the ischemia/reperfusion injury by promoting M2 macrophage polarization

Authors: Yingli Xie, Di Zhao, Pingshuan Dong, Lihong Lai*

Affiliations:

Department of Cardiology, First Affiliated Hospital of Henan University of Science and Technology, Luoyang city, Henan province 471000, China

***Corresponding to:**

Lihong Lai, Department of Cardiology, First Affiliated Hospital of Henan University of Science and Technology, Jinghua Rd, Luoyang city, Henan province 471000, China

Email: Marry_Lai@linuxmail.org

Email addresses:

Lihong Lai: Marry_Lai@linuxmail.org

Yingli Xie: Sunny_Xie@linuxmail.org

Di Zhao: Dennis_Zhao@linuxmail.org

Pingshuan Dong: Pierce_Dong@linuxmail.org

Abstract

Macrophages play essential roles in the generation and resolution of inflammation. Ischemia-reperfusion injury (IRI) triggers a systemic inflammatory response and leads to cellular injury and organ failure. During surgical procedures of the liver, such as hepatic resection and liver transplantation, IRI leads to the dysfunction of the liver. Rho-associated protein kinase (ROCK) inhibitors were reported protecting the liver from IRI. However, the systematic administration of ROCK inhibitors causes severe hypotension. Here, using Fasudil carried liposomes, we specifically inhibited the ROCK-II expression in Kupffer cells and blood monocytes. Through this macrophage/monocyte specific treatment of Fasudil, we successfully protected the liver from IRI by shifting Kupffer cells/monocytes from M1/classical to M2/patrolling phenotype in the liver and peripheral blood. Our finding provides novel insights into the macrophage/monocyte-specific drug delivery and the treatment of liver IRI.

Key Words: Fasudil, Rho-associated protein kinase, macrophage targeting, ischemia/reperfusion injury, M1/M2 macrophages

Introduction

Ischemia-reperfusion injury (IRI) is one of the most critical complications commonly associated with liver surgery [1], such as hepatic resection and liver transplantation. It comprises a sterile inflammatory response that damage organs. Macrophages/monocytes are vital in innate immunity and inflammation [2], such as phagocytosis [3,4] and resolution [5]. Macrophages/monocytes also play important roles in regulatory immunity, such as antigen presenting [4]. Recent studies showed that there are at least two types of macrophages or monocytes, M1 and M2 macrophages [6] or classical/inflammatory and patrolling/regulatory monocytes [7], respectively. M1 macrophages are the “killer” type macrophages, which promote inflammation and rapidly eliminate the pathogens but also cause tissue damage. M2 macrophages are the “heal” type macrophages, which routinely repair and maintain tissue integrity. Fasudil is a potent Rho-associated protein kinase (ROCK) inhibitor [8,9,10,11,12,13] and vasodilator and has been used for the treatment of cerebral vasospasm [9] and many other diseases, such as cancer [14,15], allergy [16] and inflammation [17,18]. The systematic administration of Fasudil was reported protecting mice from experimental autoimmune encephalomyelitis (EAE) and shifting macrophages from M1 to M2 [19]. Enhanced M2 macrophage polarization was reported to protect the liver from IRI [20]. However, the systematic administration of ROCK inhibitors, such as Fasudil, causes severe side effects, such as hypotension [21]. Thus, the specific targeting of Fasudil is needed.

Liposomes are widely used in drug delivery for macrophages/monocytes. Typically, clodronate liposomes were used to deplete various kinds of macrophage/monocyte [22,23], such as primitive macrophages [24] microglia [25], Kupffer cells [26], alveolar macrophage [27], monocytes [25], tumor-associated macrophages [28,29]. Therefore, in this study, we packaged Fasudil in liposomes to realize the specific

targeting to macrophages/monocytes. We tested the efficiency and specificity of the targeting and assessed whether the administration of Fasudil liposomes could protect the liver from IRI.

Materials and methods

Reagents

Fasudil (HA 1077, Dihydrochloride), phosphatidylcholine, cholesterol, chloroform, paraformaldehyde (PFA), Triton X-100, and Tween-200 were purchased from Sigma-Aldrich, Shanghai, China. Alexa Fluor® 488 (AF488), SYBR Gold Nucleic Acid Gel Staining and TRIzol were purchased from Thermo Fisher Scientific, Shanghai, China. Phosphate-buffered saline (PBS) was purchased from Beyotime Biotechnology, Shanghai, China. Alexa Fluor® 647 (AF647) conjugated anti-mouse F4/80 (EGF-like module-containing mucin-like hormone receptor-like 1) antibody, AF647 conjugated anti-mouse CD115 antibody, Brilliant Violet 421 (BV421) conjugated anti-mouse CD45 antibody, phycoerythrin (PE) conjugated anti-mouse Ly-6G antibody, phycoerythrin (PE) conjugated anti-mouse Ly-6C antibody, and isotype control antibodies were purchased from Biolegend, San Diego, CA, USA. PE-conjugated anti-mouse inducible nitric oxide synthase (iNOS) antibody and UltraComp eBeads were purchased from eBioscience, San Diego, CA, USA. PE-conjugated anti-mouse Arginase-1 (Arg-1) antibody was purchased from R&D system, Minneapolis, MN, USA. Rabbit anti-ROCK-II polyclonal antibody was purchased from Abcam (catalog #: ab71598), Shanghai, China. Horseradish peroxidase (HRP)-conjugated goat anti-rabbit antibody (catalog #: sc-2004), and rabbit anti-GAPDH (Glyceraldehyde 3-phosphate dehydrogenase) polyclonal antibody (catalog #: sc-25778) were purchased from Santa Cruz Biotech Inc., Santa Cruz, CA, USA. FastQuant RT Kit (with gDNase) and SuperRealPreMix Plus (SYBR Green) were purchased from Tiangen Biotech, Beijing, China. qRT-PCR primer pairs against Mus musculus gene ROCK2 was purchased from OriGene, Rockville, MD, USA. Mouse alanine aminotransferase (ALT) and aspartate aminotransferase (AST) quantitative Kits were purchased from Pointe Scientific, MI, USA.

Mouse total bilirubin (TBIL) ELISA Kits were purchased from Runyu Biotechnology, Shanghai, China. Mouse TNFα (tumor necrosis factor alpha), IL-1β (interleukin 1 beta), and IL-10 (interleukin 10) ELISA Kits were purchased from NeoBioscience, Shenzhen, China. The Liver Dissociation Kit was purchased from Miltenyi Biotec. Goat serum was purchased from Gibco, Rockville, MD, USA.

Mice

Male C57BL/6J mice were bought from the Experimental Animal Center of Henan University of Science and Technology and were used at the age of eight to ten weeks. Mice were bred and housed under specific pathogen-free conditions in groups of five mice per cage with free access to food and water. Animal breeding and experiments were conducted according to the Henan University of Science and Technology Animal Welfare guidelines and were approved by the Animal Ethics Committee of the Henan University of Science and Technology.

Preparation of liposomes

The preparation of multilamellar liposomes was assisted by Shanghai DDSome Laboratories Co., Ltd. as described before [30]. Briefly, phosphatidylcholine (86 m) and cholesterol (8 mg) were dissolved in chloroform in a round-bottom flask. After high-vacuum rotary evaporation at 37°C, the thin film that formed on the wall of the flask was dispersed by gentle shaking for 10 minutes in 10 mL of the PBS solution containing Fasudil (0.5 mg/ml) and AF488 (0.5 mg/ml). The preparations were kept for two hours at 20°C, sonicated (60 Hz) for 3 minutes at 20°C and kept at room temperature (RT) for another two hours. The liposomes were harvested by centrifuging at 10000 g for 30 minutes, were washed with

PBS, and were resuspended in 4 mL PBS. The lipid suspension was then forced through a polycarbonate filter with the successively smaller pore size (1000 nm, 500 nm, and 300 nm) mounted on a holder in a heating block (Avanti®mini-extruder). The size distribution of the liposomes was assessed by a Malvern Zetasizer Nano ZS (Malvern Instruments Ltd., UK).

Fluorescence microscopy

Liposomes carrying Fasudil and AF488 was imaged by an IX71 inverted fluorescence microscope (Olympus, Shanghai, China) equipped with a 100 × N.A. (numerical aperture) 1.45 plan-apochromatic oil immersion objective and U-LH100HG fluorescence light source. Images were captured at a rate of 0.2–1 frames per second using a 16-bit digital charge-coupled device camera (C10600-10B ORCA-R2, Hamamatsu, Beijing, China).

Liposome drug administration

Three administrations of the liposome suspension described above were applied to mice through retro-orbital intravenous (i.v.) injection (10 μL/g, 2 hours apart). One day after administrations, the efficiency and specificity of macrophage/monocyte targeting were assessed by flow cytometry. The $CD45^+F4/80^+$ or $CD45^+CD115^+$ cells were sorted to test the expression of ROCK-II. In the liver IRI experiments, surgeries were performed one day after the first three administrations, and one boost administration of the liposomes (10 μL/g) was performed every day. Liposomes without Fasudil were used as a negative control to avoid any unspecific effects for the liver IRI experiments.

Flow cytometry

During assessing the efficiency and specificity of macrophage/monocyte targeting, mice were euthanized by CO_2 inhalation. Peripheral blood and liver were harvested for the assay. The liver single-cell suspension was prepared using the Liver Dissociation Kit according to the manufacturer's instruction. Erythrocytes in the blood sample or liver cell suspension were lysed using distilled water (RT, 10 seconds). The blood sample or liver cell suspension was incubated with BV421 conjugated anti-mouse CD45 antibody (2 μg/ml) and AF647 conjugated anti-mouse CD115 antibody (2 μg/ml) or AF647 conjugated anti-mouse F4/80 antibody (1 μg/ml), respectively, for 30 minutes on ice. After two washes, cells were re-suspended in FACS buffer (0.5% BSA and 0.05% sodium azide in PBS) and were analyzed on a FACSCalibur (BD Biosciences). Compensation controls were performed using UltraComp eBeads incubated with relative antibodies at RT for 10 minutes.

For sorting of $CD115^+$ or $F4/80^+$ leukocytes from blood samples or liver cell suspensions, respectively, the cells were stained using the same method as described above and the $CD45^+CD115^+$ or $CD45^+F4/80^+$ cells were sorted on a FACSAria (BD Biosciences). The $CD115^-$ and $CD4/80^-$ cells were sorted, respectively, as controls for specific targeting.

To assess the number of neutrophils in blood and liver during IRI, we collected peripheral blood samples at different time points and harvested livers 48 hours after the surgery. Samples were prepared as described above and were stained with BV421 conjugated anti-mouse CD45 antibody (2 μg/ml) and PE-conjugated anti-mouse Ly-6G antibody (2 μg/ml) for 30 minutes on ice. After two washes, cells were re-suspended in FACS buffer (0.5% BSA and 0.05% sodium azide in PBS) and were analyzed on a FACSCalibur (BD Biosciences).

To assess the amount of classical and patrolling monocytes in blood or M1 and M2 macrophages in liver, we harvested peripheral blood samples and livers 48 hours after the surgery. Samples were prepared as described above. Blood samples were stained with BV421 conjugated anti-mouse CD45 antibody (2 μg/ml), PE-conjugated anti-mouse Ly-6C antibody (2 μg/ml), and AF647 conjugated anti-mouse CD115 antibody (2 μg/ml) for 30 minutes on ice. Intracellular staining was performed for liver single-cell suspensions: cells were fixed by 1% PFA for 10 minutes on ice, permeabilized by 0.5% Triton X-100 for one hour on ice, and treated with blocking buffer containing 2% BSA, 10% goat serum and 0.1% Tween-200 for one hour on ice. Then cells were stained with BV421 conjugated anti-mouse CD45 antibody (2 μg/ml), PE-conjugated anti-iNOS or anti-Arg-1 antibody (2 μg/ml), and AF647 conjugated anti-mouse F4/80 antibody (2 μg/ml) for 30 minutes on ice. After two washes, cells were re-suspended in FACS buffer (0.5% BSA and 0.05% sodium azide in PBS) and were analyzed on a FACSCalibur (BD Biosciences).

Flow cytometric data were analyzed using the FlowJo V9 software (FLOWJO, LLC). $CD45^+CD115^+Ly6C^{high}$ cells were defined as classical/inflammatory monocytes, $CD45^+CD115^+Ly6C^{low}$ cells were defined as patrolling/regulatory monocytes. $CD45^+F4/80^+iNOS^+$ cells were defined as M1 macrophages, $CD45^+F4/80^+Arg\text{-}1^+$ cells were defined as M2 macrophages.

Western blot

Western blot was performed as described before [19,31]. Briefly, cell lysates of sorted $F4/80^+$ or $CD115^+$ cells were fractionated by the sodium dodecyl sulfate-polyacrylamide gel electrophoresis (SDS-PAGE) and detected by immunoblotting using rabbit anti-ROCK-II polyclonal antibody (1:1000) and

HRP-conjugated goat anti-rabbit antibody (1:5000). Sample loading amounts in the assay were normalized by GAPDH (rabbit anti-mouse GAPDH polyclonal antibody, 1:2000) blotting. The blots were visualized by G:BOX Gel & Blot Imaging Systems (Syngene, Cambridge, England).

qRT-PCR

qRT-PCR was performed as described before [31]. Briefly, RNA in sorted $F4/80^+$ or $CD115^+$ cells was extracted using TRIzol. cDNA was synthesized using FastQuant RT Kit (with gDNase) according to the manufacturer's instructions. The expression level of ROCK-II, TNFα, IL-1β, and IL-10 mRNA was measured by Roche Lightcycler 480 (Roche, Nutley, NJ, USA) using SuperRealPreMix Plus (SYBR Green) and normalized to the expression level of GAPDH.

Measurement of serum ALT, AST, TBIL, TNFα, IL-1β, and IL-10

Serum ALT and AST activity were measured by mouse ALT and AST quantitative kits according to the manufacturer’s instruction. TBIL, TNFα, IL-1β, and IL-10 were measured by ELISA kits according to the manufacturer’s instruction. A Spectra MAX 190 plate reader was used for these measurements.

Cell-free DNA (cfDNA) Measurements

cfDNA was measured directly in sera using SYBR Gold Nucleic Acid Gel Staining, according to the fluorometric method published before [32,33]. Briefly, samples were added to a black 96-well plate (Greiner Bio-One). SYBR Gold was applied (1:10,000), and fluorescence was measured with a microplate fluorometer (BioTek) at an emission wavelength of 530/25 nm and an excitation wavelength

of 485/20 nm. Background fluorescence was subtracted by using sera treated with RNase A (100 U) and DNase I (500 U) for five hours at 37°C as a negative control. Commercial Salmon sperm DNA was used as DNA standards.

Partial warm liver IRI procedure

The surgical procedure was performed as described before [20,34]. Briefly, mice were fasted for 18 h before experiments and were provided with tap water ad libitum. Mice were anesthetized with ketamine (100 mg/kg, i.m.) and xylazine (10 mg/kg, i.m.). The body temperature of mice was maintained at 37 °C throughout the anesthesia process. The left branches of the portal vein and hepatic artery were clamped to induce complete ischemia of the median and left lobes of the liver. The right lobes remained perfused to prevent venous congestion of the intestine. After 60 min of ischemia, the clamp was removed to allow reperfusion. Sham-operated mice were prepared similarly; however, a clip was not placed on the vasculature leading to the median and left lobes.

Histopathology

The severity of IRI was assessed by hematoxylin and eosin (H&E) staining of liver paraffin sections. Liver specimens were fixed in formalin and then embedded in paraffin. The specimens were sectioned at 5μm and stained with H&E. Sections were scored from 0 to 4 as described before [35]. The Suzuki scores were assessed by a histopathologist blinded to the sample group.

Statistics

Statistical analysis was performed with Prism 6 (GraphPad). Data were presented as mean ± SD. The means for the data sets were compared using unpaired student t-tests with equal variances. P values less than 0.05 were considered significant.

Results

Macrophages/monocytes were specifically targeted by Fasudil carried liposomes

To realize the macrophage/monocyte specific targeting, we packaged Fasudil (Figure 1A) together with fluorescence indicator AF488 into lipid bilayer liposomes, which has been widely used in the drug delivery for macrophage/monocyte [23,26]. Size distribution measurements revealed that diameters of the produced liposomes are mainly around 300-350 nm (Figure 1B). Fluorescence imaging confirmed the liposome size and the loading of AF488 in liposomes, which indicated the loading of Fasudil in these liposomes (Figure 1C).

To test the targeting efficiency and specificity of liposomes, we used flow cytometry assay after the liposome administration. As the schematic showed in Figure 1D, when liposomes are phagocytosed by targeted cells, the fluorescence indicator AF488, which is resistant to acidity, will be carried. The targeted cells will display green fluorescence ($AF488^+$, Q1 and Q2 in Figure 1E and F), which can be detected by flow cytometry. From flow cytometry dot plots of intrahepatic leukocytes ($CD45^+$, Figure 1E), we found out that one day after the three administrations of the Fasudil/AF488 carried liposomes, most $AF488^+$ cells were Kupffer cells ($F4/80^+$, 86.61 ± 2.68%, Figure 1G) and most Kupffer cells were targeted ($AF488^+$, 86.44 ± 6.13 %, Figure 1H). Similarly, from flow cytometry dot plots of peripheral blood leukocytes ($CD45^+$, Figure 1F), most $AF488^+$ cells were monocytes ($CD115^+$, 80.85 ± 3.38 %, Figure 1G) and most monocytes were targeted ($AF488^+$, 90.95 ± 3.40 %, Figure 1H). These results demonstrated the good efficiency and specificity of the macrophage/monocyte specific drug delivery by the Fasudil/AF488 carried liposomes.

Suppressed expression of ROCK-II in macrophage/monocytes

Besides evidence that AF488 in the Fasudil/AF488 carried liposomes were specifically delivered to Kupffer cells and blood monocytes, we performed experiments to confirm the Fasudil delivery, which suppresses the expression of ROCK-II in Kupffer cells (Figure 2A, C, and E) and blood monocytes (Figure 2B, D and F). Western blot of sorted Kupffer cells ($CD45^+F4/80^+$) from liver showed a ~3/4 decreased protein expression of ROCK-II after the treatment of the Fasudil/AF488 carried liposomes (Figure 2A and C). The qRT-PCR result of these cells showed a ~1/3 decreased mRNA expression of ROCK-II after the treatment of the Fasudil/AF488 carried liposomes (Figure 2E). Similarly, in sorted monocytes ($CD45^+CD115^+$) from peripheral blood, the protein expression of ROCK-II was decreased ~3/5 (Figure 2B and D), and the mRNA expression of ROCK-II was decreased ~1/2 (Figure 2F) after the treatment of the Fasudil/AF488 carried liposomes. No significant change was found in the mRNA expression of ROCK-II in liver $F4/80^-$ cells and blood $CD115^-$ cells after the treatment of the Fasudil/AF488 carried liposomes (Figure 2G and H). This further demonstrated the targeting-specificity of the Fasudil/AF488 carried liposomes.

Fasudil carried liposomes protect liver from IRI

To assess the protecting effect of macrophage/monocyte targeting Fasudil liposomes to liver IRI, we tested ALT, AST, and TBIL concentration in serum, which reflect liver injury, in mice with surgical induction of liver IRI after the administration of liposomes or not (Figure 3A-C). Comparing to mice with sham surgery, which did not show any increase of ALT, AST, and TBIL, the concentration of ALT, AST, and TBIL all increased after liver IRI in mice with Fasudil liposome administration or not. The

administration of mock liposomes did not show any effect. In Fasudil liposome treated mice, the increase of ALT, AST, and TBIL were all significantly inhibited two hours after liver IRI. A peak concentration of less than 5,000 U/L ALT and AST was observed in Fasudil liposome treated mice, which is around three-fold less than the peak ALT and AST concentration (~15,000 and ~13,000 U/L, respectively) in liver IRI mice without liposome treatment. The TBIL concentrations continuously increased after IRI. The treatment of Fasudil liposomes significantly inhibited (about three quarters) the increase of serum TBIL. Another indicator to assess the tissue damage is cfDNA [36]. After measured the cfDNA concentration in serum (Figure 3D), we found out that in liver IRI mice, the cfDNA concentration in mice treated with Fasudil liposomes is similar to the mice without Fasudil liposome treatment in the first two hours after liver IRI. However, four hours after liver IRI, the cfDNA concentration in Fasudil liposome treat mice was decreased. A significant difference was observed in between mice treated with Fasudil liposomes or not. Sham mice do not show much cfDNA in serum. These results combined with above ALT results indicated that Fasudil liposome treatment reduced the liver tissue damage in the liver IRI mouse model. Neutrophils are vital for inflammation response [37,38] and play critical roles in IRI. During IRI, blood neutrophilia and neutrophil tissue infiltration are frequently observed [39]. Thus, we assessed the dynamics of neutrophil ($Ly6G^+$) proportion in the blood (Figure 3E) and the neutrophil ($Ly6G^+$) infiltration in liver (Figure 3F) after IRI. We found out that the administration of Fasudil liposomes can prevent neutrophilia after IRI (Figure 3E). Specifically, a severe neutrophilia was observed in liver IRI induced mice, which neutrophils continuously increased to ~80% of blood leukocytes until 24 hours after IRI. In comparison, the neutrophil percentage in mice treated with Fasudil liposomes showed an inhibited increase in the first eight hours after liver IRI and a decrease after then. The significant difference

between these two groups was observed starting at four hours after liver IRI. Sham mice did not show obvious changes in neutrophil percentage. In liver (Figure 3F), 48 hours after IRI, neutrophil infiltration in Fasudil liposome treat mice (43.68 ± 2.813 % amount all $CD45^+$ intrahepatic leukocytes) was significantly less than that in liver IRI mice without the treatment of Fasudil liposomes (70.87 ± 6.754 %). We also assessed the severity of IRI by performing H&E histology (Figure 3G and H). We found that the administration of Fasudil liposomes reduced the Suzuki scores from more than 3 to about 2 in IRI mice (Figure 3H). Overall, the inflammation after liver IRI, which is indicated by neutrophils, is inhibited by the administration of Fasudil carried liposomes. The release of inflammation cause less hepatic tissue damage and protect the liver from IRI.

Fasudil carried liposomes polarized macrophages/monocytes from M1 to M2 phenotype.

Macrophages/monocytes are key players in the modulation of immunological responses and inflammation [40,41]. The M1 or M2 macrophage phenotype is important for promoting inflammation or healing, respectively [6]. Liver IRI is a severe inflammation condition, which damages the hepatic tissue. To characterize the phenotype changes of macrophages/monocytes after IRI with or without Fasudil liposome administration, we measured the proportion of classical/inflammatory ($Ly6C^{high}$) and patrolling/regulatory ($Ly6C^{low}$) monocytes in blood leukocytes (Figure 4A-C), and M1 ($iNOS^+$) or M2 ($Arg\text{-}1^+$) Kupffer cells in intrahepatic leukocytes (Figure 4D-F) by flow cytometry.

In blood leukocytes, we found that Fasudil liposome administration significantly reduced the percentage of $Ly6C^{high}$ monocytes from ~2.7% to ~1.6% (Figure 4A) and significantly increased the percentage of $Ly6C^{low}$ monocytes from ~1.3% to ~2.3% (Figure 4B). Amount the monocyte proportion, Fasudil

liposome administration switched the inflammatory phenotype (67.5% Ly6C^{high}) to regulatory phenotype (58.4% Ly6C^{low}, Figure 4C). Forty-eight hours after the induction of liver IRI, the percentage of Ly6C^{high} monocytes increased about twice (~1.6% to ~3.0%) or more than twice (~2.7% to ~6.25%) in mice with or without Fasudil liposome treatment, respectively (Figure 4A). The percentage of Ly6C^{low} monocytes increased more than thrice (~2.3% to ~7.2%) in mice treated with Fasudil liposomes 48 hours after liver IRI. In comparison, 48 hours after liver IRI, the percentage of Ly6C^{low} monocytes significantly but slightly increased (~1.3% to ~1.8%) in mice without Fasudil liposome treatment (Figure 4B). Amount the monocyte proportion, liver IRI promoted the inflammatory phenotype (67.5% to 77.8% Ly6C^{high}) in mice without Fasudil liposome treatment but promoted the regulatory phenotype (58.4% to 70.1% Ly6C^{low}) in mice treated with Fasudil liposomes (Figure 4C). Sham mice did not show any variation of the monocyte populations.

In intrahepatic leukocytes, we found similar patterns compared to blood - Fasudil liposome administration significantly reduced the percentage of iNOS^{+} M1 Kupffer cells from ~4.6% to ~3.2% (Figure 4D) and significantly increased the percentage of Arg-1^{+} M2 Kupffer cells from ~2.4% to ~3.8% (Figure 4E). Amount the Kupffer cell proportion, Fasudil liposome administration switched the inflammatory phenotype (65.6% iNOS^{+} M1) to regulatory phenotype (54.3% Arg-1^{+} M2, Figure 4F). Forty-eight hours after the induction of liver IRI, the percentage of iNOS^{+} M1 Kupffer cells increased about trice (~4.6% to ~13.4%) in mice without Fasudil liposome treatment, but not in mice treated with Fasudil liposomes (~3.2% to ~3.8%, not significant, Figure 4D). The percentage of Arg-1^{+} M2 Kupffer cells increased more than twice (~3.8% to ~9.6%) in mice treated with Fasudil liposomes 48 hours after liver IRI. In comparison, 48 hours after liver IRI, the percentage of Arg-1^{+} M2 Kupffer cells significantly but mildly increased (~2.4%

to ~3.5%) in mice without Fasudil liposome treatment (Figure 4E). Amount the Kupffer cell proportion, liver IRI promoted the inflammatory phenotype (65.6% to 70.2% Ly6C^{high}) in mice without Fasudil liposome treatment but promoted the regulatory phenotype (54.3% to 71.6% Ly6C^{low}) in mice treated with Fasudil liposomes (Figure 4F). Sham mice did not show any variation of the monocyte populations.

Fasudil carried liposomes lead to a shift in cytokine expression profiles.

To assess the cytokine expression after the treatment of Fasudil carried liposomes in liver IRI, we measured the amount of pro-inflammatory cytokines TNFα and IL-1β and anti-inflammatory cytokine IL-10 in the serum of IRI mice treated with liposomes with or without Fasudil. Sham mice treated with mock liposomes were used as controls. We found that the IRI of liver induced a predominant increase of TNFα (Figure 5A) and IL-1β (Figure 5B) compared to sham controls. The macrophage/monocyte targeting Fasudil treatment significantly inhibited the increase of serum TNFα and IL-1β in mice with the liver IRI. Mice with the liver IRI showed an increase of serum IL-10 (Figure 5C) compared to sham controls. This increase is significantly boosted by the treatment of Fasudil-carrying liposomes in mice with the liver IRI. The treatment of control liposomes did not affect the cytokine amount in serum of mice with the liver IRI.

We also tested mRNA expression of these cytokines in sorted Kupffer cells (CD45^{+}F4/80^{+}) using qRT-PCR. Similar to serum cytokines, we found out that the mRNA expressions of TNFα, IL-1β, and IL-10 in Kupffer cells were increased in mice with the liver IRI compared to sham controls (Figure 5D-F). The treatment of Fasudil-carrying liposomes resulted in a significantly lower mRNA expression of TNFα (Figure 5D) and IL-1β (Figure 5E) but a significantly higher mRNA expression of IL-10 (Figure 5F) in

Kupffer cells compared to those in liver IRI mice without treatments. The treatment of control liposomes did not affect the cytokine expression in Kupffer cells of mice with the liver IRI.

Discussion

In this study, we specifically targeted macrophages/monocytes by packaging Fasudil in liposomes. Efficiency and specificity of the targeting were confirmed by the gain-of-fluorescence of macrophages/monocytes from the co-packaged AF488 indicator. The ROCK-II inhibition in macrophages/monocytes was demonstrated by reduced protein and mRNA expression. The polarization from M1 to M2 phenotype in blood monocytes and Kupffer cells was established by flow cytometry assay. These shift from inflammatory to regulatory phenotype reduced the inflammatory responses – neutrophilia in blood and neutrophil infiltration in hepatic tissue, resulting in a protective effect of liver from IRI.

Many attempts have been made to protect the liver from IRI. Most of them are based on regulating the M1/M2 macrophage responses. IL-10, an important chemokine which can enhance M2 macrophage polarization, was demonstrated to protect the liver from IRI [42]. iNOS inhibitor, which can inhibit M1 macrophage response, was reported as having a curative effect in liver IRI [43]. Resolvin D1, which is an endogenous pro-resolving lipid mediator, was reported to polarizing macrophage to M2 phenotype and inhibit liver IRI [20]. ROCK inhibitors were showed a protective effect in liver IRI in the previous study [44,45]. But they thought that effect is hepatic stellate cell dependent. ROCK is a kinase belonging to the AGC (PKA/ PKG/PKC) family of serine-threonine kinases. ROCK is a key regulator of actin organization and thus a regulator of cell migration [46]. The function of ROCK in macrophage regulation

is contradictory [19,47]. Our studies demonstrated that ROCK inhibitor could polarize macrophage to M2 phenotype and protect the liver from IRI. Because our study is the first to use a method specific targeting macrophages/monocytes, we may conclude that the previous studies, which showed decrease M2 macrophage after ROCK inhibitor treatment, might be an indirect effect caused by the systematic administration.

List of abbreviations used

IRI: Ischemia-reperfusion injury; ROCK: Rho-associated protein kinase; PFA: Paraformaldehyde; PBS: Phosphate-buffered saline; AF: Alexa Fluor®; BV: Brilliant Violet; PE: Phycoerythrin; iNOS: inducible nitric oxide synthase; Arg-1: Arginase-1; HRP: Horseradish peroxidase; GAPDH: Glyceraldehyde 3-phosphate dehydrogenase; ALT: Alanine aminotransferase; AST: Aspartate aminotransferase; TBIL: total bilirubin; RT: Room temperature; FACS: Fluorescence-activated cell sorting; SDS-PAGE: Sodium dodecyl sulfate polyacrylamide gel electrophoresis; qRT-PCR: quantitative real-time polymerase chain reaction; cfDNA: cell-free DNA; SD: Standard deviation; TNFα: tumor necrosis factor alpha ; IL-1β: interleukin 1 beta; IL-10: interleukin 10; EAE: Experimental autoimmune encephalomyelitis.

Declarations:

Ethics approval and consent to participate

Animal breeding and experiments were conducted according to the Henan University of Science and Technology Animal Welfare guidelines and were approved by the Animal Ethics Committee of the Henan University of Science and Technology.

Consent to publish

Not applicable

Availability of data and materials

All contributing authors agree and declare that the data and material is available by contacting the corresponding author L.L.

Competing interests

All contributing authors declare that they have no conflict of interest.

Funding

Not applicable

Authors' Contributions

Experiments were designed by Y.X. and L.L. Experiments were performed by Y.X., D.Z., and P.D. Data analysis was performed by Y.X. The manuscript was written by Y.X. and L.L. The project was supervised by L.L. All authors (Y.X., D.Z., P.D. and L.L.) discussed the results and revised the manuscript.

Acknowledgements

We thank the technicians from the animal facilities in the First Affiliated Hospital of Henan University of Science and Technology for their assistance on animal cares.

References:

[1] M. Zhu, B. Lu, Q. Cao, Z. Wu, Z. Xu, W. Li, X. Yao, F. Liu, IL-11 Attenuates Liver Ischemia/Reperfusion Injury (IRI) through STAT3 Signaling Pathway in Mice, PLoS One 10 (2015) e0126296.

[2] E. Galkina, K. Ley, Leukocyte influx in atherosclerosis, Curr Drug Targets 8 (2007) 1239-1248.

[3] D.W. Shim, K.H. Heo, Y.K. Kim, E.J. Sim, T.B. Kang, J.W. Choi, D.W. Sim, S.H. Cheong, S.H. Lee, J.K. Bang, H.S. Won, K.H. Lee, Anti-Inflammatory Action of an Antimicrobial Model Peptide That Suppresses the TRIF-Dependent Signaling Pathway via Inhibition of Toll-Like Receptor 4 Endocytosis in Lipopolysaccharide-Stimulated Macrophages, PLoS One 10 (2015) e0126871.

[4] M.M. Barrio, R. Abes, M. Colombo, G. Pizzurro, C. Boix, M.P. Roberti, E. Gelize, M. Rodriguez-Zubieta, J. Mordoh, J.L. Teillaud, Human macrophages and dendritic cells can equally present MART-1 antigen to CD8(+) T cells after phagocytosis of gamma-irradiated melanoma cells, PLoS One 7 (2012) e40311.

[5] S. Khanna, S. Biswas, Y. Shang, E. Collard, A. Azad, C. Kauh, V. Bhasker, G.M. Gordillo, C.K. Sen, S. Roy, Macrophage dysfunction impairs resolution of inflammation in the wounds of diabetic mice, PLoS One 5 (2010) e9539.

[6] C.D. Mills, K. Ley, M1 and M2 macrophages: the chicken and the egg of immunity, J Innate Immun 6 (2014) 716-726.

[7] B.I. Mitchell, M.M. Byron, R.C. Ng, D.C. Chow, L.C. Ndhlovu, C.M. Shikuma, Elevation of Non-Classical (CD14+/lowCD16++) Monocytes Is Associated with Increased Albuminuria and Urine TGF-beta1 in HIV-Infected Individuals on Stable Antiretroviral Therapy, PLoS One 11

(2016) e0153758.

[8] D.S. Whitlon, M. Grover, S.F. Dunne, S. Richter, C.H. Luan, C.P. Richter, Novel High Content Screen Detects Compounds That Promote Neurite Regeneration from Cochlear Spiral Ganglion Neurons, Sci Rep 5 (2015) 15960.

[9] C.M. Mikelis, M. Simaan, K. Ando, S. Fukuhara, A. Sakurai, P. Amornphimoltham, A. Masedunskas, R. Weigert, T. Chavakis, R.H. Adams, S. Offermanns, N. Mochizuki, Y. Zheng, J.S. Gutkind, RhoA and ROCK mediate histamine-induced vascular leakage and anaphylactic shock, Nat Commun 6 (2015) 6725.

[10] C. Li, G. Zhen, Y. Chai, L. Xie, J.L. Crane, E. Farber, C.R. Farber, X. Luo, P. Gao, X. Cao, M. Wan, RhoA determines lineage fate of mesenchymal stem cells by modulating CTGF-VEGF complex in extracellular matrix, Nat Commun 7 (2016) 11455.

[11] L. Truebestein, D.J. Elsner, E. Fuchs, T.A. Leonard, A molecular ruler regulates cytoskeletal remodelling by the Rho kinases, Nat Commun 6 (2015) 10029.

[12] Y. Kaneko, M. Ohta, T. Inoue, K. Mizuno, T. Isobe, S. Tanabe, H. Tanihara, Effects of K-115 (Ripasudil), a novel ROCK inhibitor, on trabecular meshwork and Schlemm's canal endothelial cells, Sci Rep 6 (2016) 19640.

[13] A. Sharanek, A. Burban, M. Burbank, R. Le Guevel, R. Li, A. Guillouzo, C. Guguen-Guillouzo, Rho-kinase/myosin light chain kinase pathway plays a key role in the impairment of bile canaliculi dynamics induced by cholestatic drugs, Sci Rep 6 (2016) 24709.

[14] H. Ying, S.L. Biroc, W.W. Li, B. Alicke, J.A. Xuan, R. Pagila, Y. Ohashi, T. Okada, Y. Kamata, H. Dinter, The Rho kinase inhibitor fasudil inhibits tumor progression in human and rat tumor

models, Mol Cancer Ther 5 (2006) 2158-2164.

[15] J. Wang, K. Hu, J. Guo, F. Cheng, J. Lv, W. Jiang, W. Lu, J. Liu, X. Pang, M. Liu, Suppression of KRas-mutant cancer through the combined inhibition of KRAS with PLK1 and ROCK, Nat Commun 7 (2016) 11363.

[16] J. Han, Y. Yi, C. Li, Y. Zhang, L. Wang, Y. Zhao, C. Pan, A. Liang, Involvement of Histamine and RhoA/ROCK in Penicillin Immediate Hypersensitivity Reactions, Sci Rep 6 (2016) 33192.

[17] Z. Ma, J. Zhang, R. Du, E. Ji, L. Chu, Rho kinase inhibition by fasudil has anti-inflammatory effects in hypercholesterolemic rats, Biol Pharm Bull 34 (2011) 1684-1689.

[18] D. Kentrup, S. Reuter, U. Schnockel, A. Grabner, B. Edemir, H. Pavenstadt, O. Schober, M. Schafers, E. Schlatter, E. Bussemaker, Hydroxyfasudil-mediated inhibition of ROCK1 and ROCK2 improves kidney function in rat renal acute ischemia-reperfusion injury, PLoS One 6 (2011) e26419.

[19] C. Liu, Y. Li, J. Yu, L. Feng, S. Hou, Y. Liu, M. Guo, Y. Xie, J. Meng, H. Zhang, B. Xiao, C. Ma, Targeting the shift from M1 to M2 macrophages in experimental autoimmune encephalomyelitis mice treated with fasudil, PLoS One 8 (2013) e54841.

[20] J.W. Kang, S.M. Lee, Resolvin D1 protects the liver from ischemia/reperfusion injury by enhancing M2 macrophage polarization and efferocytosis, Biochim Biophys Acta 1861 (2016) 1025-1035.

[21] S. Etienne-Manneville, A. Hall, Rho GTPases in cell biology, Nature 420 (2002) 629-635.

[22] Z. Li, X. Xu, X. Feng, P.M. Murphy, The Macrophage-depleting Agent Clodronate Promotes Durable Hematopoietic Chimerism and Donor-specific Skin Allograft Tolerance in Mice, Sci Rep 6 (2016) 22143.

[23] J. GUO, Z. FAN, Z. GU, X. WEI, STUDYING THE ROLE OF MACROPHAGES IN CIRCULATING PROSTATE CANCER CELLS BY IN VIVO FLOW CYTOMETRY, Journal of Innovative Optical Health Sciences 05 (2012) 1250027.

[24] J. Travnickova, V. Tran Chau, E. Julien, J. Mateos-Langerak, C. Gonzalez, E. Lelievre, G. Lutfalla, M. Tavian, K. Kissa, Primitive macrophages control HSPC mobilization and definitive haematopoiesis, Nat Commun 6 (2015) 6227.

[25] J. Peng, N. Gu, L. Zhou, B.E. U, M. Murugan, W.B. Gan, L.J. Wu, Microglia and monocytes synergistically promote the transition from acute to chronic pain after nerve injury, Nat Commun 7 (2016) 12029.

[26] C.L. Elsegood, C.W. Chan, M.A. Degli-Esposti, M.E. Wikstrom, A. Domenichini, K. Lazarus, N. van Rooijen, R. Ganss, J.K. Olynyk, G.C. Yeoh, Kupffer cell-monocyte communication is essential for initiating murine liver progenitor cell-mediated liver regeneration, Hepatology 62 (2015) 1272-1284.

[27] T. Bouchery, R. Kyle, M. Camberis, A. Shepherd, K. Filbey, A. Smith, M. Harvie, G. Painter, K. Johnston, P. Ferguson, R. Jain, B. Roediger, B. Delahunt, W. Weninger, E. Forbes-Blom, G. Le Gros, ILC2s and T cells cooperate to ensure maintenance of M2 macrophages for lung immunity against hookworms, Nat Commun 6 (2015) 6970.

[28] M.A. Miller, Y.R. Zheng, S. Gadde, C. Pfirschke, H. Zope, C. Engblom, R.H. Kohler, Y. Iwamoto, K.S. Yang, B. Askevold, N. Kolishetti, M. Pittet, S.J. Lippard, O.C. Farokhzad, R. Weissleder, Tumour-associated macrophages act as a slow-release reservoir of nano-therapeutic Pt(IV) pro-drug, Nat Commun 6 (2015) 8692.

[29] Y. Yang, P. Andersson, K. Hosaka, Y. Zhang, R. Cao, H. Iwamoto, X. Yang, M. Nakamura, J. Wang, R. Zhuang, H. Morikawa, Y. Xue, H. Braun, R. Beyaert, N. Samani, S. Nakae, E. Hams, S. Dissing, P.G. Fallon, R. Langer, Y. Cao, The PDGF-BB-SOX7 axis-modulated IL-33 in pericytes and stromal cells promotes metastasis through tumour-associated macrophages, Nat Commun 7 (2016) 11385.

[30] N. Van Rooijen, A. Sanders, Kupffer cell depletion by liposome-delivered drugs: comparative activity of intracellular clodronate, propamidine, and ethylenediaminetetraacetic acid, Hepatology 23 (1996) 1239-1243.

[31] Z. Fan, X. Cui, D. Wei, W. Liu, B. Li, H. He, H. Ye, N. Zhu, X. Wei, eEF1A1 binds and enriches protoporphyrin IX in cancer cells in 5-aminolevulinic acid based photodynamic therapy, Scientific Reports 6 (2016) 25353.

[32] A. Avriel, M. Paryente Wiessman, Y. Almog, Y. Perl, V. Novack, O. Galante, M. Klein, M.J. Pencina, A. Douvdevani, Admission cell free DNA levels predict 28-day mortality in patients with severe sepsis in intensive care, PLoS One 9 (2014) e100514.

[33] H. Goldshtein, M.J. Hausmann, A. Douvdevani, A rapid direct fluorescent assay for cell-free DNA quantification in biological fluids, Ann Clin Biochem 46 (2009) 488-494.

[34] Z.C. Fan, J. Yan, G.D. Liu, X.Y. Tan, X.F. Weng, W.Z. Wu, J. Zhou, X.B. Wei, Real-time monitoring of rare circulating hepatocellular carcinoma cells in an orthotopic model by in vivo flow cytometry assesses resection on metastasis, Cancer Res 72 (2012) 2683-2691.

[35] S. Suzuki, S. Nakamura, T. Koizumi, S. Sakaguchi, S. Baba, H. Muro, Y. Fujise, The beneficial effect of a prostaglandin I2 analog on ischemic rat liver, Transplantation 52 (1991) 979-983.

[36] Y. Xin, X. Gao, W. Wang, X. Xu, L. Yu, X. Ju, A. Li, Circulating cell-free DNA indicates M1/M2 responses during septic peritonitis, Biochem Biophys Res Commun 477 (2016) 589-594.

[37] Z. Fan, S. McArdle, Z. Mikulski, E. Gutierrez, B. Engelhardt, U. Deutsch, M. Ginsberg, A. Groisman, K. Ley, Neutrophil recruitment limited by high affinity bent β2 integrin binding ligand in cis, Nature Communications in press (2016).

[38] Z. Fan, K. Ley, Developing Neutrophils Must Eat...Themselves!, Immunity 47 (2017) 393-395.

[39] Z.V. Schofield, T.M. Woodruff, R. Halai, M.C. Wu, M.A. Cooper, Neutrophils--a key component of ischemia-reperfusion injury, Shock 40 (2013) 463-470.

[40] M. Bosma, M. Gerling, J. Pasto, A. Georgiadi, E. Graham, O. Shilkova, Y. Iwata, S. Almer, J. Soderman, R. Toftgard, F. Wermeling, E.A. Bostrom, P.A. Bostrom, FNDC4 acts as an anti-inflammatory factor on macrophages and improves colitis in mice, Nat Commun 7 (2016) 11314.

[41] T.H. Tran, R. Rastogi, J. Shelke, M.M. Amiji, Modulation of Macrophage Functional Polarity towards Anti-Inflammatory Phenotype with Plasmid DNA Delivery in CD44 Targeting Hyaluronic Acid Nanoparticles, Sci Rep 5 (2015) 16632.

[42] J.D. Ellett, C. Atkinson, Z.P. Evans, Z. Amani, E. Balish, M.G. Schmidt, N. van Rooijen, R.G. Schnellmann, K.D. Chavin, Murine Kupffer cells are protective in total hepatic ischemia/reperfusion injury with bowel congestion through IL-10, J Immunol 184 (2010) 5849-5858.

[43] C.M. Hsu, J.S. Wang, C.H. Liu, L.W. Chen, Kupffer cells protect liver from ischemia-reperfusion injury by an inducible nitric oxide synthase-dependent mechanism, Shock 17 (2002) 280-285.

[44] S. Kuroda, H. Tashiro, Y. Kimura, K. Hirata, M. Tsutada, Y. Mikuriya, T. Kobayashi, H. Amano, Y. Tanaka, H. Ohdan, Rho-kinase inhibitor targeting the liver prevents ischemia/reperfusion injury in the steatotic liver without major systemic adversity in rats, Liver Transpl 21 (2015) 123-131.

[45] S. Kuroda, H. Tashiro, Y. Igarashi, Y. Tanimoto, J. Nambu, A. Oshita, T. Kobayashi, H. Amano, Y. Tanaka, H. Ohdan, Rho inhibitor prevents ischemia-reperfusion injury in rat steatotic liver, J Hepatol 56 (2012) 146-152.

[46] K. Riento, A.J. Ridley, Rocks: multifunctional kinases in cell behaviour, Nat Rev Mol Cell Biol 4 (2003) 446-456.

[47] A. Zanin-Zhorov, R. Flynn, S.D. Waksal, B.R. Blazar, Isoform-specific targeting of ROCK proteins in immune cells, Small GTPases 7 (2016) 173-177.

Figure Legends:

Figure 1. Targeting macrophages and monocytes by the Fasudil/AF488 carried liposomes. (A) Chemical structure of Fasudil. (**B**) Size distribution of the Fasudil/AF488 carried liposomes. (**C**) A representative epi-fluorescence image of the Fasudil/AF488 carried liposomes. The scale bar is 5 μm. (**D**) Schematic showing the macrophage (Mφ) targeting by the Fasudil/AF488 carried liposomes (L). Macrophages and monocytes are the main phagocytes in individuals. By uptake the Fasudil/AF488 carried liposomes through phagocytosis, the macrophages/monocytes will be specifically treated with Fasudil and labeled with the AF488. (**E-F**) Representative flow cytometry dot plots showing the targeting efficiency of the $F4/80^+$ Kupffer cells (**E**) and $CD115^+$ monocytes (**F**) in liver and blood, respectively, assessed by flow cytometry one day after the intravenous injection of the Fasudil/AF488 carried liposomes. Mice injected with mock liposomes were used as the control. (**G**) Targeting efficiency: Bar graphs showed the average percentage of targeted $AF488^+$ cells in $F4/80^+$ Kupffer cells and $CD115^+$ monocytes in liver and blood, respectively, from three individual experiments. Mean ± SD. *$p<0.05$. (**H**) Targeting specificity: Bar graphs showed the average percentage of $F4/80^+$ Kupffer cells and $CD115^+$ monocytes in targeted $AF488^+$ cells in liver and blood, respectively, from three individual experiments. Mean ± SD. *$p<0.05$.

Figure 2. Fasudil/AF488 carried liposomes inhibit the expression of ROCK-II in macrophages and monocytes. (**A-D**) Western blot showed the suppressed expression of ROCK-II in the sorted $F4/80^+$ Kupffer cells (**A** and **C**) and $CD115^+$ blood monocytes (**B** and **D**) after the Fasudil targeting. **C** and **D**

showed the quantitative results from three individual experiments. The ROCK-II expression was normalized by GADPH expression. Mean ± SD. *p<0.05. (**E-H**) qRT-PCR showed the suppressed expression of ROCK-II in the sorted F4/80^{+} Kupffer cells (**E**), CD115^{+} blood monocytes (**F**), F4/80^{-} non-Kupffer liver cells (**G**), and CD115^{-} non-monocyte blood cells (**H**) after the Fasudil targeting from three individual experiments. Mean ± SD. *p<0.05. n.s. means no significance, p>0.05.

Figure 3. Macrophage targeted treatment of Fasudil protects the liver from ischemia/reperfusion injury. (**A-D**) Dynamic changes of the serum alanine transaminase (ALT, **A**), aspartate aminotransferase (AST, **B**), total bilirubin (TBIL, **C**), and cell-free DNA (cfDNA, **D**) after the liver ischemia/reperfusion injury (IRI) with or without the administration of the Fasudil/AF488 carried liposomes (Fasudil Lipo). (**E-F**) Macrophage-targeted treatment of Fasudil prevent the neutrophilia (**E**) and neutrophil liver infiltration (**F**) after the liver ischemia/reperfusion injury. Mice with sham surgery were served as a negative control. (**G-H**) Histopathological assessment of IRI. Typical H&E images (**G**) of Sham, IRI, IRI + Fasudil liposomes, and IRI + control liposomes were presented, respectively. Scale bars are all 200 μm. The Suzuki scores (**H**) were assessed by a histopathologist blinded to the sample group. n = 6 per group. Mean ± SD. *p<0.05 when compared the Fasudil Lipo group vs. IRI group.

Figure 4. Fasudil-targeting shifts blood monocytes and hepatic macrophage from classical to patrolling and M1 to M2 phenotype, respectively, in the liver ischemia/reperfusion injury (IRI). (**A-B**) Percentage of classical/inflammatory (CD115^{+}Ly6C^{high}, **A**) and patrolling/regulatory (CD115^{+}Ly6C^{low}, **B**) monocytes in the blood leukocytes before and twelve hours after the liver IRI with or without the administration of the

Fasudil/AF488 carried liposomes (Fasudil Lipo), or with the administration of control liposomes without Fasudil. Mice with sham surgery were served as a negative control. n = 6 per group. Mean ± SD. *p<0.05. **C.** The pie chart showed the $Ly6C^{high}$ vs. $Ly6C^{low}$ balance in blood monocytes. (**D**-**E**) Percentage of M1 ($F4/80^{+}iNOS^{+}$, **D**) and M2 ($F4/80^{+}$ $Arg\text{-}1^{+}$, **E**) macrophages in the hepatic leukocytes before and twelve hours after the liver IRI with or without the administration of the Fasudil liposomes, or with the administration of control liposomes. Mice with sham surgery were served as negative control. n = 6 per group. Mean ± SD. *p<0.05. (**F**) The pie chart showed the $iNOS^{+}$ vs. $Arg\text{-}1^{+}$ balance in hepatic macrophages.

Figure 5. Fasudil-targeting shifts cytokine expression from pro-inflammation to anti-inflammation in the liver ischemia/reperfusion injury (IRI). (**A**-**C**) The amount of pro-inflammatory cytokines TNFα (**A**) and IL-1β (**B**), as well as the anti-inflammatory cytokine IL-10 (**C**) in the serum of liver IRI mice treated with or without Fasudil liposomes (Fasudil Lipo or IRI, respectively). (**D**-**F**) mRNA expressions of TNFα (**D**), IL-1β (**E**), and IL-10 (**F**) in the sorted CD45+F4/80+ Kuppfer cells from livers of IRI mice treated with or without Fasudil liposomes (Fasudil Lipo or IRI, respectively). IRI mice treated with mock liposomes were used as a control (Control Lipo). Mice with sham surgery were served as a negative control. n = 6 per group. Mean ± SD. *p<0.05 when compared the Fasudil Lipo group vs. IRI group.

Figure 1

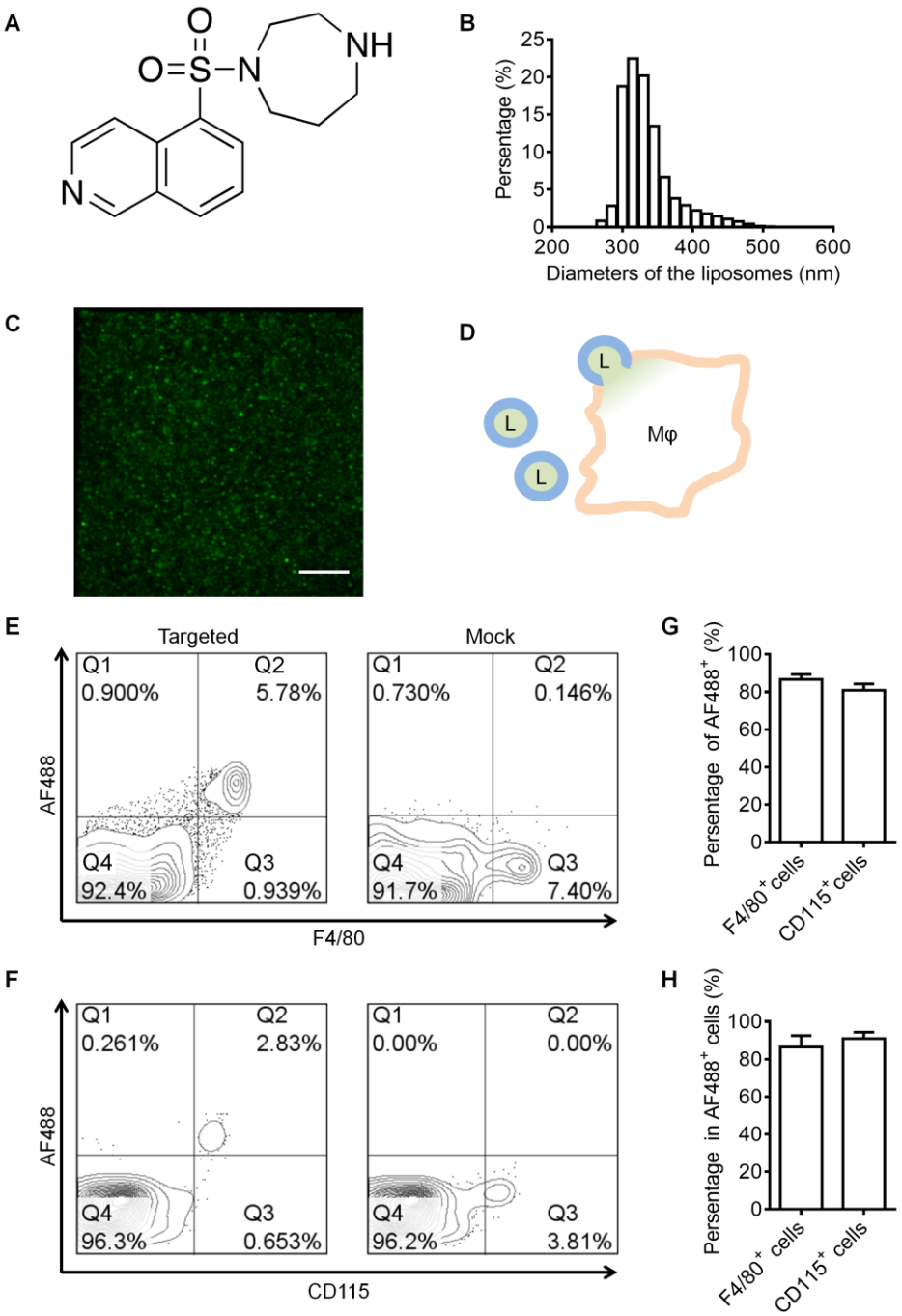

Figure 2

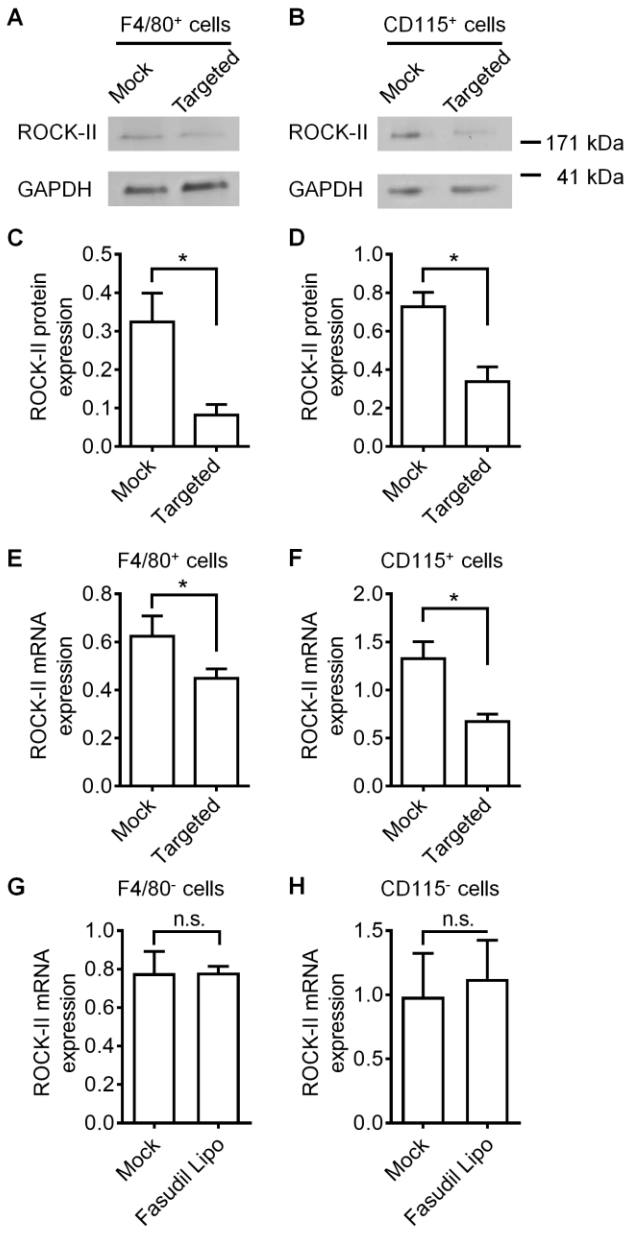

Figure 3

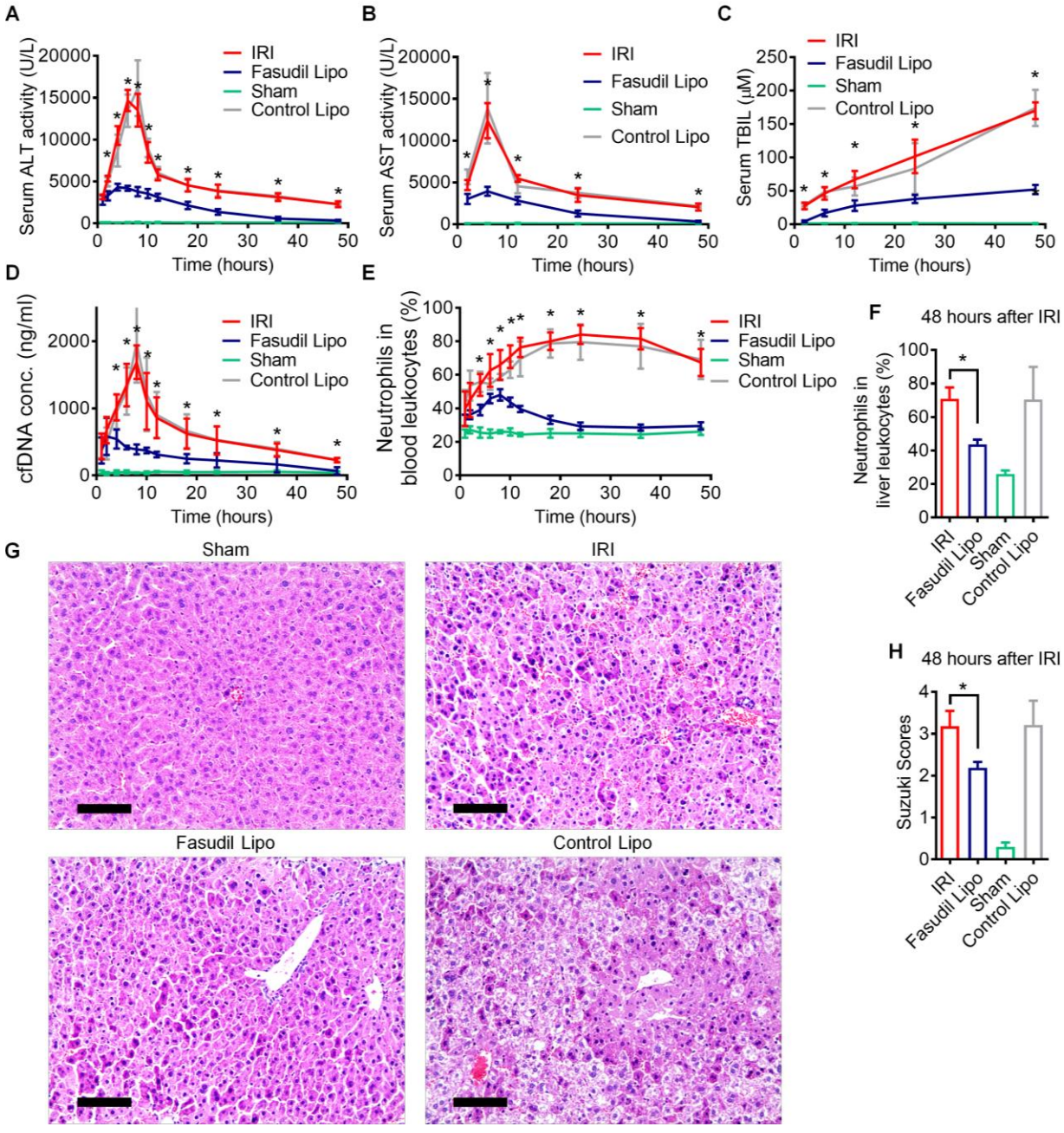

Figure 4

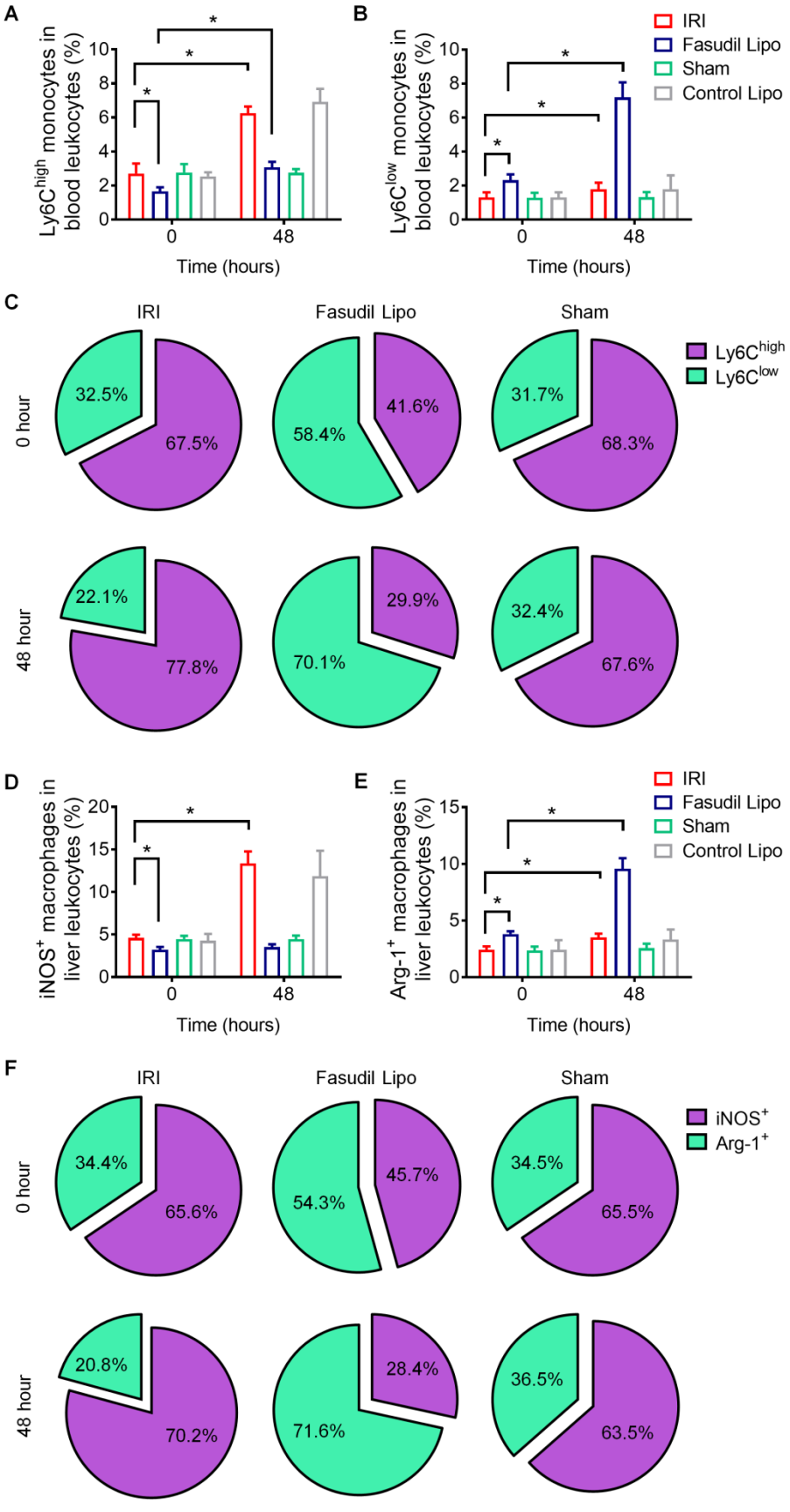

Figure 5